

RECPAD 2016

22nd Portuguese Conference on
Pattern Recognition

Aveiro, Portugal
October 28th, 2016

Program Committee Chair

Armando J. Pinho

Organizing Committee

Armando J. Pinho
Diogo Pratas
Raquel Sebastião
Samuel Silva
Sónia Gouveia
Susana Brás

Secretariat

Anabela Viegas

Organized by

IEETA — Institute of Electronics and Informatics Engineering of Aveiro
DETI — Department of Electronics, Telecommunications and Informatics
University of Aveiro

In cooperation with

APRP — Associação Portuguesa de Reconhecimento de Padrões

Contents

Preface	9
Keynote	11
Program Committee	13
Poster Session I	17
Why should you model time when you use Markov Models for heart sound analysis	17
<i>Jorge Oliveira, Theofrastos Mantadelis and Miguel Coimbra</i>	
Tracking of the Anterior Mitral Leaflet in Echocardiographic Sequences using Active Contours	19
<i>Malik Saad Sultan, Nelson Martins and Miguel Coimbra</i>	
Pedestrian Detection Using Multi-Stage Features in Fast R-CNN	21
<i>Miguel Farrajota, João Rodrigues and J.M.H Du Buf</i>	
Image Segmentation and Classification for the Location of Tumors and Other Diseases	23
<i>Ana Rodrigues, Carmen Nunes, Verónica Vasconcelos and Micael Couceiro</i>	
Multi-modal Image Registration for Generation of Complete 3D Models of the Breast: A Technical Review	25
<i>Sílvia Bessa, Jaime Cardoso and Hélder Oliveira</i>	
Compression Methods on Emotion Identification - Preliminary Study	27
<i>Susana Brás, Jacqueline Ferreira, Sandra C. Soares and Armando Pinho</i>	
A simple Net for a Deep Problem - Emotion Recognition	29
<i>Ana Laranjeira, Bernardete Ribeiro, Xavier Frazão and André Pimentel</i>	
Landmines detection using thermal infrared sensors	31
<i>Jorge Leitão Pimenta, José Silvestre Silva and José Bioucas-Dias</i>	
Discriminative Directional Classifiers: Logistic Regression and K-Nearest Neighbors	33
<i>Kelwin Fernandes and Jaime Cardoso</i>	
Predicting Student Performance with Data from an Interactive Learning System	35
<i>Ana Gonçalves, Ana Tomé and Luís Descalço</i>	
Motion Recognition from Accelerometer, Gyroscope and ECG Data	38
<i>Soraya Sinche, Bernardete Ribeiro and Jorge Sá Silva</i>	
Multi-Object Tracking with Distributed Sensing	40
<i>Ricardo Dias, Nuno Lau, João Silva and Gi Hyun Lim</i>	
Facial recognition based on image compression	43
<i>Marco Henriques, António J. R. Neves and Armando Pinho</i>	
Using Deep Machine Learning for Medical Image De-identification	45
<i>Eriksson Monteiro, Carlos Costa and José Luis Oliveira</i>	
Poster Session II	49
Parametric Modeling of Breast Data Using Free Form Deformation	49
<i>Hooshiar Zolfagharnasab, Jaime S. Cardoso and Hélder P. Oliveira</i>	

Psychophysiology assessment tool using Virtual Reality - Case Study	51
<i>Bernardo Marques, Susana Brás, Sandra Soares and José Maria Fernandes</i>	
Facial Key-Points Detection using a Convolutional Encoder-decoder Model	53
<i>Pedro M. Ferreira, Jaime S. Cardoso and Ana Rebelo</i>	
Epileptic Seizure Prediction with univariate EEG features and Stacked AutoEncoders	55
<i>Ricardo Barata, Bernardete Ribeiro, António Dourado and César Teixeira</i>	
Boosting Compression-based Classifiers for Authorship Attribution	57
<i>Filipe Teixeira and Armando Pinho</i>	
Detection of small juxta-pleural nodules in computed tomography images	59
<i>Guilherme Aresta, António Cunha and Aurélio Campilho</i>	
Deriving ECG to compute inhalation during to fire experiments	61
<i>Raquel Sebastião, Sandra Sorte, Joana Valente, Ana I. Miranda and José M. Fernandes</i>	
Mixed-Integer Programming Model for the Discovery of Disease Biomarkers Profiles	63
<i>André M. Santiago, Miguel Rocha and Joel P. Arrais</i>	
A practical study about the Google Vision API	66
<i>Daniel Lopes and António J. R. Neves</i>	
Estimation of choroidal thickness in OCT images	68
<i>Simão P. Faria, Susana Penas, Luís Mendonça, Jorge A. Silva and Ana Maria Mendonça</i>	
Segmentation of the Left Ventricle in Cardiac MRI using a Robust Active Shape Model Approach	71
<i>Carlos Santiago, Jacinto Nascimento and Jorge S. Marques</i>	
A System for the Analysis of Dermoscopy Images Using Weak Annotations	73
<i>Catarina Barata, M. Emre Celebi and Jorge S. Marques</i>	
Irregularity Detection in ECG signal using a semi-fiducial method	75
<i>João Carvalho, Armando Pinho and Susana Brás</i>	
Machine Learning with Word Embeddings applied to Biomedical Concept Disambiguation ..	77
<i>Rui Antunes and Sérgio Matos</i>	
Poster Session III	81
Intrinsic Page Hinkley Test (iPHT)	81
<i>Raquel Sebastião and José Maria Fernandes</i>	
Pattern Recognition in Images of Counterfeited Documents	83
<i>Rafael Vieira, Catarina Silva, Mário Antunes and Ana Assis</i>	
Segmentations of Vascular Networks: A Technological Review	85
<i>Ricardo J. Araújo, Jaime S. Cardoso and Hélder P. Oliveira</i>	
Vessel width estimation in eye fundus images	87
<i>Teresa Araújo, Ana Maria Mendonça and Aurélio Campilho</i>	
Human Pose Estimation Using Wide Stacked Hourglass Networks	89
<i>Miguel Farrajota, João Rodrigues and Hans Du Buf</i>	
Semantic Modelling for User Interaction with Sonic Content	91
<i>António Sá Pinto, Matthew Davies and Perfecto Herrera</i>	
Twitter classification: are some examples better than others?	93
<i>Joana Costa, Catarina Silva, Mário Antunes and Bernardete Ribeiro</i>	
Dynamic Recognition of Obstacles for Optimal Robot Navigation	95
<i>Miguel Fernandes and Luís A. Alexandre</i>	
Initial validation of online ECG signal segmentation	97
<i>Tiago J. O. Magalhães, José Maria Fernandes, Ilídio Castro Oliveira and Susana Brás</i>	
Anomaly-based intrusion detection using application-specific traffic profiles	99
<i>Hassan Alizadeh and André Zúquete</i>	

Mobile Application in the Executive Function Assessment of Parkinson’s Disease	101
<i>Tiago Fonseca, Sofia Pires, Verónica Vasconcelos and Emília Bigotte</i>	
Pre-trained ConvNet models as feature extractors and label estimators: A comparative study in large datasets	103
<i>John Cebola and Luís Teixeira</i>	
Single nucleotide variation context in human genome	105
<i>Vera Enes, João Manuel Rodrigues and Vera Afreixo</i>	
Directional Outlyingness applied to distances between Genomic Words	108
<i>Ana Tavares, Vera Afreixo, Paula Brito and Peter Filzmoser</i>	

Estimation of choroidal thickness in OCT images

Simão P. Faria³Susana Penas⁴Luís Mendonça⁵Jorge A. Silva^{2,3}Ana Maria Mendonça^{1,3}

1- Dep. of Electrical and Computer Eng., Faculty of Engineering, University of Porto

2- Dep. of Informatics Engineering, Faculty of Engineering, University of Porto

3- INESC TEC, Porto

4- Dep. of Ophthalmology, São João Hospital Center

5- Dep. of Ophthalmology, Hospital of Braga

Abstract

The choroid is the middle layer of the eye globe located between the retina and the sclera. It is proven that choroidal thickness is a sign of multiple eye diseases. Optical Coherence Tomography (OCT) is an imaging technique that allows the visualization of tomographic images of near surface tissues like those in the eye globe. The automatic calculation of the choroidal thickness reduces the subjectivity of manual image analysis as well as the time of large scale measurements.

In this paper, a method is presented for the automatic estimation of the choroidal thickness in OCT images. The pre-processing of the images is focused on noise reduction, shadow removal and contrast adjustment. The inner and outer boundaries of the choroid are delineated sequentially, resorting to a minimum path algorithm. The choroidal thickness is given by the distance between the two boundaries.

The method was evaluated by calculating the error as the absolute distance from the automatically estimated outer boundaries to the boundaries delineated by two ophthalmologists, in 14 images. The differences between the two sets of manual boundaries are usually larger than the error of the automatic segmentation.

Usually OCT scans are performed in two perpendicular sets, allowing a comparison of the segmentation of one set with the other, after alignment and interpolation. The differences in choroidal thickness measured from each set have a median of approximately 2.2% of the average thickness.

1 Introduction

The choroid is the middle layer of the eye globe located between the retina and the sclera (Figure 1), bordered internally by the Bruch's Membrane (BM) and externally by the Choroidal-Scleral Interface (CSI). Its purpose is to provide metabolic needs to the retina and to regulate ocular pressure and temperature[3]. The vascular nature of the choroid makes the variations of its thickness an indication for the ocular health. Pathologies as retinitis pigmentosa, serous chorioretinopathy, diabetic retinopathy and others that cause inflammation in the tissue may induce the thickening of the choroid, while the narrowing can be associated with myopia, dehydration or age [2].

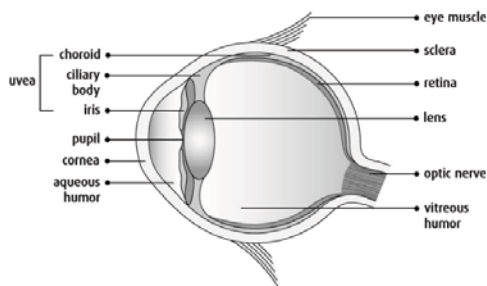


Figure 1: Anatomical model of the eye (image source:[4]).

The OCT is a non-invasive, non-painful, fast imaging technique that can get information unavailable through other imaging methods. This tomographic technique enables the *in vivo* visualization of subsuperficial tissues with high resolution. Developing software tools to help physicians get the most of this recent technique will certainly contribute for the health of multiple patients.

Recent technological advances in the optical OCT, allowed a better visualization of deeper structures such as the CSI, so the automatic segmentation of the choroid becomes more viable [2].

2 Methods

2.1 Automatic Segmentation

In order to estimate the thickness of the choroid, its two boundaries, the BM and the CSI, must be detected (Figure 2). An additional curve, named Interdigitation Zone (IZ), corresponding to a hyperreflective layer inside the retina (Figure 2) must also be detected, in a preliminary step. This curve is used as a reference for the delineation of the BM. In the

The IZ, BM and CSI curves are determined using a minimum cost path algorithm (MCPA) [3], based on a cost function that depends on the characteristics of the curve to delineate. This cost function is expressed by a cost matrix that has the size of the image it is generated from.

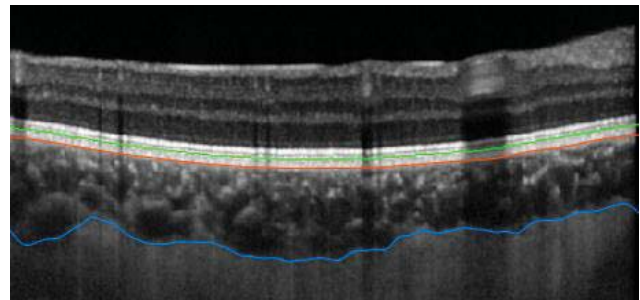


Figure 2: OCT image with the detected curves: Interdigitation Zone (IZ), in green; Bruch's Membrane (BM), in orange; and Choroidal-Scleral Interface (CSI), in blue. The choroid is delimited by BM and CSI.

In a first step, the contrast of the image is adjusted by raising the value of each pixel to the fourth power [4]. This allows an enhancement of the brighter areas of the retina (Figure 3.a) that is fundamental for the detection of the IZ.

The cost matrix for the delineation of the IZ, using the MCPA, is obtained by calculating the negative image of a smoothed version of the contrast adjusted image [1]. An average filter, with 60 by 55 μm , is used for the smoothing, that agrees with the normal thickness of the brightest region in the healthy eye (approximately 60 μm).

The estimation of the IZ will aid the location of the BM. The cost matrix for the delineation of the BM incorporates two penalty terms: one for paths that are far away from the IZ and another one for paths above the IZ. On the other way, a term is included in the cost matrix that favours the curves that are in the transition from the brighter layers of the retina to the darker choroidal tissue; this term is based on the value of a Sobel derivative [3].

After delineating the BM, another contrast compensation algorithm is applied to the image. The objective of this processing is to compensate for the loss of the signal energy in the ocular tissue and to deal with the shadows cast by retinal vessels [1][3]. The resulting image (Figure 3.b) has a better contrast in the CSI region; however the speckle noise is enhanced.

The following step is the flattening and cropping of the image [3] (Figure 3.c). The flattening is done by shifting every column of the image so that the BM becomes a horizontal straight line. Cropping is done by cutting the image 515 μm below the BM; this height guarantees that the choroid is included in the cropped image. This step is made to limit the path search to a region of interest.

In order to reduce the noise and attenuate the shadows, before the delineation of the CSI, a stationary wavelet transform is applied. A five level wavelet decomposition is done, using a Haar wavelet [5], and a hard threshold is applied to the horizontal coefficients of the decomposition. By setting this threshold to zero, the resulting image has less horizontal details, which helps to attenuate shadows (Figure 3.d) and keeps the intensity of the vertical transitions between the choroid and the sclera.

Finally, to delineate the CSI, the cost matrix used in the MCPA is based on the sum of two components that favour paths in the transition between the darker parts of the choroid and the lighter sclera. The first one is computed by applying a morphological opening (to remove the white parts of the choroid) with an 80 by 60 μm kernel, followed by Gaussian smoothing and vertical derivative computation, with a vertical length of 512 μm . The second one uses the same kind of smoothing and derivative computation, but with a smaller kernel, for a fine localization, and is only defined in the dark-to-light transitions identified by the first component [1]. The use of two kernels allows a good spatial

discrimination without a great impact of the choroidal vessels and noise that can have the same type of transitions as the CSI and generate errors.

The thickness of the choroid is calculated as the mean vertical distance between the BM and the CSI.

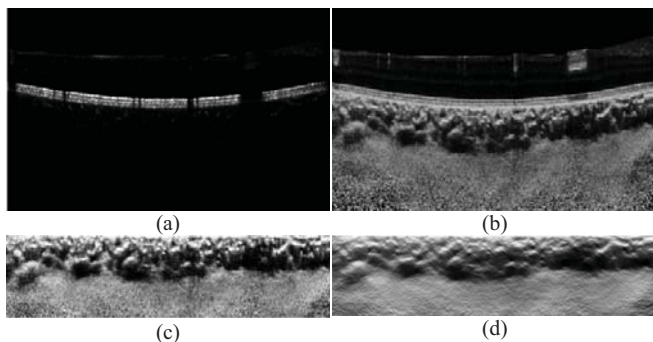


Figure 3: OCT image after: (a) contrast adjustment; (b) compensation algorithm; (c) flattening and cropping; (d) wavelet based filtering.

2.2 Merging sets of B-scans

Usually two sets of OCT scans are acquired for the same eye, in perpendicular directions. Each set consists of 49 parallel B-scans, covering a rectangular area. Figure 4 shows two infrared (IR) images of the fundus of an eye, where the covered area is signalled; the arrowed line indicates the position and the direction of one of the acquired B-scans



Figure 4: Examples of the IR images with the location of the B-scans.

It is possible to improve the thickness measures by using the information obtained from both sets. However, originally they are not anatomically aligned. An image registration algorithm is used in order to align the IR images. The algorithm based in the maximization of mutual information by translating and rotating the images (Figure 5). The resulting transformation matrix is used for the alignment of the B-scan data.

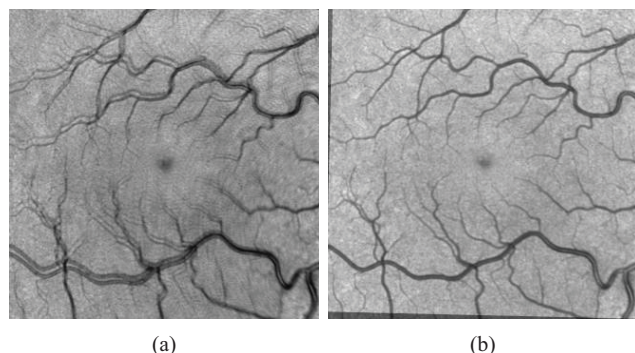


Figure 5: Example of the overlapping IR images that represent the area scanned by the OCT. (a) original IR images of two OCT videos of the same eye are merged in one representation; (b) the IR images are aligned using the image registration algorithm.

For the comparison between measures obtained from the two sets, an interpolated 3D surface representing the CSI is obtained for each set. This surface is sampled at each one of the positions of the orthogonal B-scans, obtaining interpolated CSI boundaries that can be compared with the boundaries detected in those orthogonal scans (Figure 6).

The comparison of the surfaces obtained from the two orthogonal scans allowed an additional evaluation of the algorithm's precision.

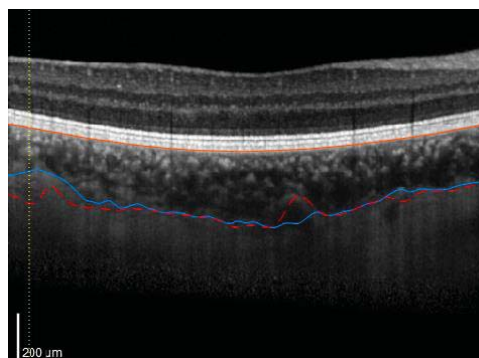


Figure 6: Example of an OCT B-scan with plots of the choroidal boundaries. In orange, the BM; in blue the CSI; the dotted red line represents the interception of the CSI membrane calculated using the series of B-scans in the perpendicular direction; the yellow dotted line locates the maximum difference between the blue and the dotted red lines.

3 Results and Discussion

To evaluate the performance of the automatic delineation of the CSI, the results of the algorithm were compared with manual markings delineated by two ophthalmologists, in 14 OCT images (7 horizontal and 7 vertical) of a single eye. This also allowed an analysis of the interobserver variability.

As observable in Figure 7, there are situations where the similarity between the three markings is clearly visible (Figure 7.a) and others where even the manual markings have discrepancies in certain zones (Figure 7.b) caused by the inclusion of vessels from the proximal sclera.

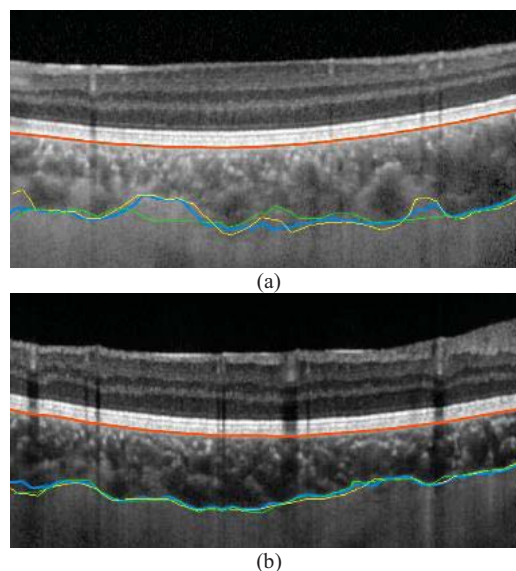


Figure 7: OCT images with the automatically detected BM (orange) and CSI (blue), and the two manual markings (yellow and green).

Results show that the errors for the automatic segmentation are comparable to the differences between the manual paths. The average errors are $12.3 \pm 12.6 \mu\text{m}$ and $12.6 \pm 13.7 \mu\text{m}$, for each one of the ophthalmologists' markings. These errors are lower than the average difference between the two manual paths: $14.4 \pm 16.5 \mu\text{m}$.

The 3D interpolated CSI boundaries, were used for the calculation of the differences between the choroidal thicknesses estimated from each set of B-scans. The histogram of the differences (Figure 8) shows that they are predominantly small. The mean absolute difference is approximately 11.49 μm and the median is 6.45 μm , meaning that the majority of differences are smaller than 2.2% of the average choroidal thickness of the analyzed eye (288.54 μm).

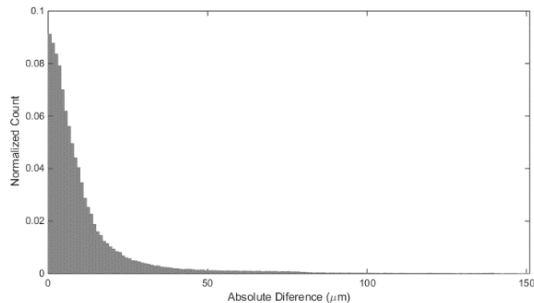


Figure 8: Histogram of the values of the thickness differences between the two sets of B-scans. The normalized count is the number of points divided by the total number of common points.

The differences in thickness measured from the two orthogonal sets can be caused by the way some vessels are sectioned in the tomographic image: in one direction they may seem as part of the choroid while in the other they may seem as scleral vessels. This kind of errors can also cause an incorrect manual delineation, because in common OCT analysis, the ophthalmologist does not make this kind of comparison between different sets of B-scans.

In the developed software application, the CSI interface obtained from each set is shown to the user, who has the possibility of manually correcting the automatic delineations.

4 Conclusion

A method for automatically estimating the choroidal thickness in OCT images was described. The choroidal thickness was calculated by detecting the internal and external boundaries (the BM and the CSI).

The dataset of OCT images allowed an interpolation of the delineated boundaries to obtain 3D surfaces. It was possible to align the B-scans and compare the segmentations in two orthogonal directions.

The final results of the automatic choroidal segmentation were very adequate. The errors in the position of the automatic boundaries are lower than the differences between the two manual markings made by physicians.

The developed software was tested on 98 B-scans. In future development of this work, the robustness of this algorithm should be evaluated using a larger set with ground truth BM and CSI boundaries, from different patients.

Acknowledgements

This work is supported by Project "NanoSTIMA: Macro-to-Nano Human Sensing: Towards Integrated Multimodal Health Monitoring and Analytics/NORTE-01-0145-FEDER-000016", financed by the North Portugal Regional Operational Programme (NORTE 2020), under the PORTUGAL 2020 Partnership Agreement, and through the European Regional Development Fund (ERDF).

References

- [1] S. P. Faria, "Estimation of choroidal thickness in OCT images," Faculty of Engineering, University of Porto, 2016.
- [2] A. González-López, B. Remeseiro, M. Ortega, and M. G. Penedo, "Choroid characterization in EDI OCT retinal images based on texture analysis," *ICAART 2015 - 7th Int. Conf. Agents Artif. Intell. Proc.*, vol. 2, pp. 269–276, 2015.
- [3] D. Alonso-Caneiro, S. A. Read, and M. J. Collins, "Automatic segmentation of choroidal thickness in optical coherence tomography.," *Biomed. Opt. Express*, vol. 4, no. 12, pp. 2795–812, Dec. 2013.
- [4] "<http://www.cancer.ca/en/cancer-information/cancer-type/eye/anatomy-and-physiology/?region=on>," accessed on Sep 2016.
- [5] H. Danesh, R. Kafieh, H. Rabbani, and F. Hajizadeh, "Segmentation of choroidal boundary in enhanced depth imaging OCTs using a multiresolution texture based modeling in graph cuts," *Comput. Math. Methods Med.*, vol. 2014, Article ID 479268, 9 pages, 2014.